 FDMP, vol.4, no.1, pp.43-54, 2008

Subcritical and Oscillatory Dynamic Surface Deformations in Non-Cylindrical Liquid Bridges

V. Shevtsova[1,2], A. Mialdun[1], C. Ferrera[1,4], M. Ermakov[3]
M. G. Cabezas[4] and J. M. Montanero[4]

Abstract: Dynamic free surface deformations induced by buoyant and thermocapillary convection in liquid bridges of $5\,cSt$ silicone oil are studied experimentally and numerically. The experiments are performed in ground conditions and static deformation is unavoidable. Convective motion starts in the liquid bridge as soon as $\Delta T \neq 0$ and initially leads to a stationary dynamic deformation of the free surface. Oscillatory motion starts at a critical value of ΔT and causes oscillations of the interface. The final supercritical shape of the free surface is a result of the static shape with superimposed subcritical stationary and oscillatory dynamic deformations. All these contributions are strongly influenced by the initial volume of the liquid bridge. The study was performed in three steps for different initial volumes: (1) the static shape was measured experimentally and the physical properties of liquid were fine-tuned by comparing the measured shape with the computed one; (2) subcritical deformations due to stationary convection were studied numerically; (3) supercritical dynamic deformations due to oscillatory convection were measured experimentally.

Keyword: dynamic surface deformation, oscillation, liquid bridge, experiment, optical technique.

[1] MRC, CP-165/62, Université Libre de Bruxelles, 50, av. F. D. Roosevelt,B-1050 Brussels, Belgium
[2] Corresponding author; e-mail: vshev@ulb.ac.be
[3] Institute for Problems in Mechanics RAS,101 Vernadsky Avenue, Bldg 1, 119526 Moscow Russia
[4] Departamento de Electrónica e Ingeniería Electromecánica, Universidad de Extremadura, E-06071 Badajoz, Spain

1 Introduction

The temperature variation along the interface induces thermocapillary stresses which cause bulk motion. A great number of studies has been conducted over the last decades devoted to the hydrodynamic stability of thermocapillary convection as it relates to the float-zone crystal-growth process. The float zone is commonly analyzed by a half-zone model, when a drop of a liquid is kept by surface tension between two differently heated rods. The thermocapillary flow arises as soon as a tiny temperature difference ΔT is applied between supporting rods. At ground conditions this flow is modified by the buoyancy force. The relative importance of buoyancy to thermocapillary effect is determined by the so called dynamic Bond number, which is the ratio of the Rayleigh number, Ra, and the Marangoni number, Ma. The convective flow causes a dynamic free surface deformation.

The free surface shape is controlled by the characteristic capillary (σ_0/d), hydrostatic $(\rho g d)$ and hydrodynamic $(\sigma_T \Delta T/d)$ pressures, and the viscous force per unit area $P_{scale} = \rho V_{scale}^2 = \rho(\nu/d)^2$. Here the magnitude of the static deformation of the interface depends on the static Bond number which is the ratio of the hydrostatic to the capillary pressure:

$$Bo_{st} = \frac{(\rho g d)}{(\sigma_0/d)} = \frac{\rho g d^2}{\sigma_0} \tag{1}$$

Here ρ is the density, ν is the kinematic viscosity, σ_0 is the surface tension at reference temperature, $\sigma_T = d\sigma/dT$, and d is the length scale.

The experimental studies of the hydrothermal stability in statically deformed liquid bridges were much more advanced then theoretical developments, e.g. Hu et al. (1994), Shevtsova et al.

(1999), Sumner et al. (2001). The first theoretical work considering half-zones with a free surface deformation was the two-dimensional calculation by Shevtsova & Legros (1998) assuming static free surface position. Later on a number of 3D computational studies of thermocapillary and buoyant flows in liquid bridges appears which assumed statically deformed interface, see for example Chen & Hu (1998), Lappa et al. (2001), Nienhüser & Kuhlmann (2002), Sim & Zebib (2002), Ermakov & Ermakova (2004),Shevtsova (2005).

The Capillary number provides a measure of the magnitude of dynamic free surface deformations. One may define the Capillary number in two different manners: Ca as the ratio of the hydrodynamic pressure to the typical capillary pressure or C as the ratio of the viscous force per unit area to the typical capillary pressure. These Capillary numbers are coupled through the Reynolds number

$$Ca = \frac{(\sigma_T \Delta T/d)}{(\sigma_0/d)} = \frac{\sigma_T \Delta T}{\sigma_0}, \tag{2}$$

$$C = \frac{(\rho \nu^2/d^2)}{(\sigma_o/d)} = \frac{\rho \nu^2}{\sigma_0 d}, \qquad Ca = C \cdot Re \tag{3}$$

In most liquid bridge experiments $C \ll 1$ and $Ca < 1$. The small value of the Capillary number, Ca, corresponds to the case of small surface tension variation as compared to the mean surface tension and thus the dynamic free surface deformations can be neglected. The first attempt to capture dynamic free surface deformations in liquid bridges was reported by Shevtsova et al. (1997). Two-dimensional calculations for small capillary numbers $Ca \ll 1$ with $Pr = 105$ showed that the amplitude of interface oscillations is very small and is only about 1% of the static shape. They obtained that the amplitude of the free surface oscillation varied along the axial coordinate and depends on the initial volume of the liquid.

Kuhlmann & Nienhuser (2002) performed a detailed 3D linear stability analysis of the dynamic free-surface deformations in liquid bridges with $Pr = 0.02$ and $Pr = 4.38$ using an asymptotic expansion in the limit $Ca \to 0$. Dynamic deformations caused by steady axisymmetric flows and by

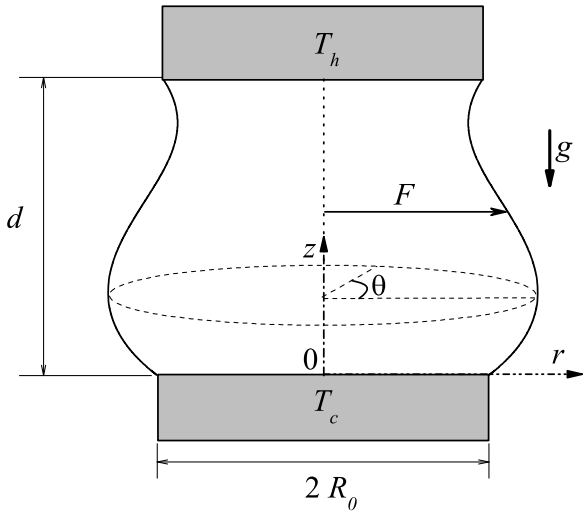

Figure 1: Sketch and coordinate system of the liquid bridge

time-dependent three dimensional critical modes were examined.

The role of the dynamic deformation in the mechanism of instability is still under discussion. Kamotani et al. (2000, 2007) advocates an idea that dynamic deformation is important in the development of instability for high Prantdl fluid. They argue that the main driving force is confined at the small region near the hot corner and it is possible disturb the region significantly even by small free surface deformations. Theoretical results, performed in asymptotic limit $Ca \to 0$, show that surface deformations are caused by lower order flow fields. Thus dynamic deformations do not feed back to the leading order thermocapillary flow.

Obviously, there is a lack of experimental results. The existence of free surface oscillations above the critical point was experimentally demonstrated by Shu et al. (1994) using an optical technique. Nishino & Yoda (2000) reported that the maximal value of amplitude of oscillations is about $1\mu m$ in experiments with $5cSt$ silicone oil.

A comprehensive experimental study of the shape and amplitude of dynamic interface oscillations was recently conducted by Ferrera et al. (2007) in a liquid bridge filled with $5cSt$ silicone oil ($Pr \approx 68$). The free surface shape was determined

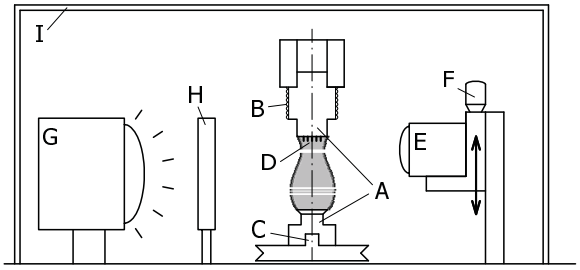

Figure 2: Experimental set-up: rods (A), heating element (B), cooling system (C), thermocouples (D), video camera (E), micrometer screw (F), optic fiber (G), diffuser (H), plexiglass box (I).

by silhouette measurements. Temperature oscillations inside the liquid bridge were also recorded by five thermocouples. Comparing the dynamic behavior of temperature and amplitude of oscillations the authors drew the conclusion that the non-linear dynamics of flow is well described by the free surface oscillations.

The present paper is the further development of the previous experimental study by Ferrera et al. (2007). One of the major goals is to examine the shape and dynamic behavior of free surface oscillations in subcritical and oscillatory regimes of thermo-capillary and buoyant convection.

2 Experimental

The experiments are performed in ground conditions and static deformation is unavoidable. Convective motion starts in the liquid bridge as soon as $\Delta T \neq 0$ and initially leads to a stationary dynamic deformation of the free surface. Oscillatory motion starts at a critical value of ΔT and causes oscillations of the interface. The final supercritical shape of the free surface is a result of the static shape with superimposed subcritical stationary and oscillatory dynamic deformations. The static shape can be measured by the proposed technique with good accuracy and the physical properties of liquid can be fine-tuned by comparison of measured shape with numerical one, calculated according Young-Laplace equation. In the case of dynamic shape analysis our attention is focused on measurement of the oscillation amplitude.

2.1 Set-up

A small volume of $5cSt$ silicone oil is held between two coaxial rods of radius $R_0 = 3.0mm$ placed a distance $d = 3.7mm$ apart as shown in Fig. 1. The lateral free surface is described by a function of the vertical coordinate $F = F(z,t)$, which measures the distance between a surface element and the liquid bridge axis (the z axis).

The sketch of the experimental arrangement is shown in Fig. 2. The rods (A) are made from aluminum alloy (with a thermal conductivity of 164 W/m K) and lateral sides are coated with Fluorad FC-723 to prevent liquid creeping over the edges. A heating element (B) (Minco electrical resistance of 100 Ohms) was mounted around the upper rod while the lower rod was connected to a thermoregulated water cooling system (C).

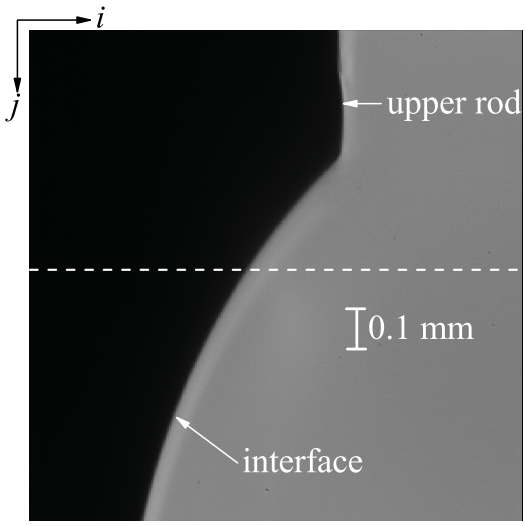

Figure 3: A digital image of the liquid bridge interface close to the upper rod

The liquid bridge was formed by injecting liquid from a regulated push syringe (syringe infusion pump KDS200) which enabled measuring the liquid volume with high accuracy. Temperature oscillations due to time-dependent convection were measured by inserting 5 shielded thermocouples (D) of 0.25 mm diameter inside the liquid at the same height $z = 1.26$ mm and radial position $r = 2.2$ mm, and with an azimuthal angle displacement of 72°.The temperature signals

Table 1: Physical properties of 5cSt silicone oil ($25°C$)

ν	β	σ	α	$d\sigma/dT$	ρ
m^2/s	$1/K$	N/m	m^2/s	N/mK	kg/m^3
$5\cdot10^{-6}$	$1.09\cdot10^{-3}$	$1.97\cdot10^{-2}$	$7.31\cdot10^{-8}$	$-6.37\cdot10^{-5}$	912.

from the thermocouples were amplified and bandpass filtered before being recorded by a computer at time intervals of 0.1 s.

Digital images were taken using a CCD camera (E) with optical lens providing a frame covering an area of about 0.809×0.809 mm. Digital images of 1004×1004 pixels were acquired during the experiment at 45 frames per second and recorded by the computer. The camera was displaced vertically during the experiment using a micrometer screw (F) for image acquisition along the whole liquid bridge. Another micrometer screw allowed horizontal translation to focus the liquid bridge contour. The liquid bridge was illuminated from the back side by cool white light provided by an optic fiber (G) connected to a light source. The light crossed a diffuser (H). The whole system (liquid bridge cell, camera, optical lens, ...) was mounted on a fixed platform and surrounded by a Plexiglas box (I) to protect against ambient-air disturbances. The measurements procedure is described elsewhere, e.g. Ferrera et al. (2007).

2.2 Processing of data

The results presented hereafter were mainly obtained from the measurement in the first field of view, i.e. near the upper hot corner.

Figure 3 shows a digital image of the interface close to the upper rod. The amplitude of the interface oscillations is much smaller than the pixel size ($0.806\ \mu m$) in many of the cases analyzed, and thus the position of the liquid bridge contour must be determined *at the sub-pixel level*.

Mathematically, a digital image is defined by the grey intensity matrix $I(i,j)$, which takes an integer value between 0 (black) and 255 (white) for each pixel (i,j), where i and j correspond to the horizontal and vertical directions, respectively. Ideally, the interface should correspond to a step in the grey intensity in the direction perpendicular to the interface. However, in real images the intensity change smears out over several pixels. Different approaches were analyzed for more precise determination of the interface position and preference was given to the criterion based on thresholding, i.e. the separation of light and dark regions. Among this class, global thresholding techniques was chosen, see Ferrera et al. (2006). This method is adequate for processing images of uniformly illuminated objects, which is the case in the present study. Comparison of the local and global thresholding techniques reveals the difference about two pixels in the determination of the interface position. Nevertheless, this discrepancy is not relevant when calculating the amplitude and frequency of the oscillation.

Following the thresholding technique, time dependence of the interface position for fixed values of z are obtained. The distance $R_0 - F(z;t)$ between the interface position and the cylindrical shape was measured as a function of the distance $\Delta z \equiv d - z$ from the top solid support. The amplitudes and characteristic frequencies are obtained from either a non-linear fitting procedure or a Fourier analysis, depending on the shape of the oscillations.

Temperature oscillations inside the liquid bridge are also recorded by five thermocouples. All temperature signals given by the thermocouples were amplified and bandpass filtered before being recorded by a computer at time intervals of 0.1 s. The characteristic frequencies are determined applying the Fourier analysis to records of temperature on large time interval.

3 Numerical solutions

3.1 Formulation of the problem

As it was mentioned above, the present experimental set-up allows us to determine the displacement of the interface with great accuracy while sub-critical liquid-gas position can be evaluated

up to the constant of a few microns depending on the method.

For this reason the dynamic surface deformations were numerically calculated. The two-dimensional calculations in cylindrical geometry were performed in sub-critical parameter space, $\Delta T < \Delta T_{cr}$. The motion of the liquid is induced by thermo-capillary effect and by buoyancy force. The surface tension acting on the free surface and the density are assumed linearly decreasing functions of the temperature:

$$\sigma(T) = \sigma_0(T_c) - \sigma_T(T - T_c), \tag{4}$$

$$\rho(T) = \rho_0(T_c) - \beta_T(T - T_c), \tag{5}$$

where $\sigma_T = -(d\sigma/dT)|_{T_c}$, $\beta = -1/\rho_0(d\rho/dT)$. The governing equations, describing stationary states, are the momentum, energy and continuity equations for an incompressible Newtonian fluid in the Boussinesq approximation

$$[\partial_t + \mathbf{V}\cdot\nabla]\,\mathbf{V} = -\frac{1}{\rho}\nabla P + \nu\nabla^2\mathbf{V} + \beta g(T - T_o)\mathbf{e}_z, \tag{6}$$

$$[\partial_t + \mathbf{V}\cdot\nabla]\,T = \kappa\nabla^2 T, \tag{7}$$

$$\nabla\cdot\mathbf{V} = 0, \tag{8}$$

where the velocity, pressure and temperature are denoted as $\mathbf{V}$, T and P. Here ν is the kinematic viscosity and κ is the thermal diffusivity.

The stress balance between the viscous fluid and the inviscid gas on the non-flat free surface $r = F(z,t)$ is given by

$$[P - P_o + \sigma(\nabla\cdot\mathbf{n})]\,\mathbf{n}_i = \mathbf{S}_{ik}\mathbf{n}_k + \tau_\mathbf{i}\cdot\nabla\sigma \tag{9}$$

where $\mathbf{S}_{ik} = \mu(\partial V_i/\partial x_k + \partial V_k/\partial x_i)$ is the viscous stress tensor, P and P_o, are the liquid and ambient gas pressures, and $\sigma(\nabla\cdot\mathbf{n})$ is the Laplace pressure.

The dimensionless parameters appearing in the governing equations and boundary conditions (except defined earlier in Eqs. 1-3) are: the Prandtl, Grashof, surface Reynolds and dynamic Bond numbers as well as the aspect and volume ratios:

$$Pr = \frac{\nu}{k},\quad Gr = \frac{g\beta\Delta T d^3}{\nu^2},\quad Re = \frac{\sigma_T\Delta T d}{\rho_0\nu^2},$$
$$Bo_{dyn} = \frac{Gr}{Re} = \frac{g\rho\beta d^2}{\sigma_T},\quad \Gamma = \frac{d}{R_0},\quad \mathscr{V} = \frac{V}{\pi R_0^2 d} \tag{10}$$

3.2 Solution method

The moving boundary problem Eq. 6–Eq. 9 can be solved by perturbation methods in the asymptotic limit of small Capillary numbers $Ca, C \to 0$, assuming that $O(Ca) \approx O(C)$. The following expansions are used to find the leading order contributions to the flow and temperature fields:

$$f(r,z,t) = f_0(r,z,t) + C\,f_1(r,z,t) + O(C^2),$$
$$\tilde{P} = C^{-1}P_{st} + P_0 + C\,P_1 + O(C^2), \tag{11}$$
$$\tilde{h}(h,t) = h_0(z) + C\,h_1(z,t) + O(C^2)$$

Here $f(r,z,t)$ reads for the components of velocity vector $\mathbf{V}$ and the temperature T, and the dimensionless free surface $h(z,t) = F(z,t)/R_0$.

The perturbation method splits the solution in a few steps: first the shape of interface is accurately determined in a static configuration; then the complete moving boundary problem transforms into a convection problem with the previously calculated free-surface location. At the next point dynamic surface deformations are determined from the flow field computed in the previous step.

The numerical code, which was used in previous studies, e.g. Shevtsova et al. (1997), Shevtsova (2005) was adapted to the present experimental system. Here we just mention some key points of the solution method. The static free surface shape is calculated by solving the Young-Laplace equation at the prescribed static Bond number, aspect ratio, and volume.

Body-fitted curvilinear coordinates were employed for solving the Navier-Stokes and energy equations. The original physical domain of non-rectangular cross section (liquid bridge with deformed interface) was transformed into a rectangular computational domain. On this rectangular domain the two-dimensional discretized equations are solved directly by iterative Newton-Raphson procedure with optimal choice of the

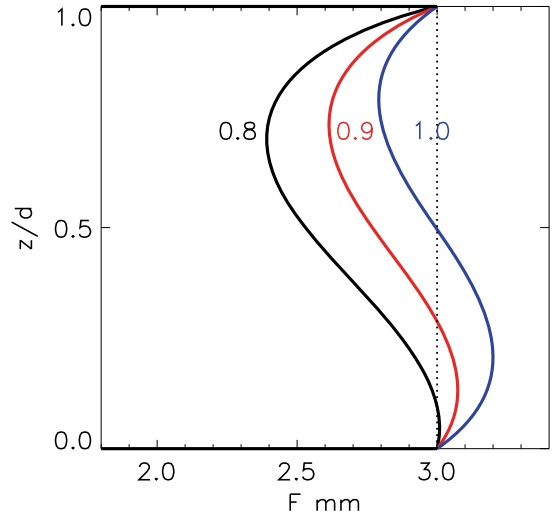

Figure 4: Static shapes ($\Delta T = 0$) for different volumes of the liquid bridge: $\mathscr{V} = 0.8, 0.9, 1.0$ when $Bo_{st} = 6.25$ and $\Gamma = 1.23$; dashed line indicates $F = R_0$.

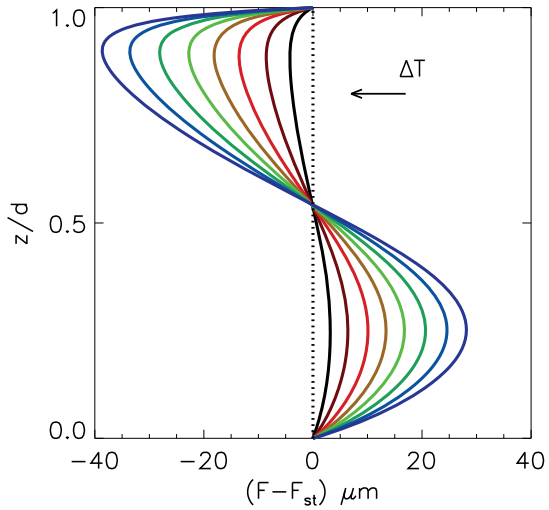

Figure 5: The evolution of dynamic surface deformations with the increasing ΔT for $\mathscr{V} = 0.8$

relaxation parameter. The steady-solution is obtained by convergence of the transient calculations. Calculations were performed on a non-uniform staggered grid $[161 \times 161]$.

3.3 Subcritical dynamic deformations

Parameter settings are selected to match the experiments including gravity (Gr) and to allow dynamic free-surface deformation (Ca, C). The temperature independent parameters are the Prandtl number, $Pr = 68$, and aspect ratio $\Gamma = 1.23$. In agreement with the experimental runs, the calculations were done for 3 different volumes of liquid bridge, $\mathscr{V} = 0.8,\ 0.9,\ 1.0$. Reynolds, Grashof numbers as well as Bond and Capillary numbers, are functions of ΔT. The flow solutions, static and dynamic deformations of the free surface were calculated for wide range of temperature differences $\Delta T = 0.,\ 2.5,\ 5.0,\ 7.5,\ 10.0,\ 12.5,\ 15.0,\ 17.5,\ 20.0 K$. To determine the static shape the new values of Bond and Capillary numbers were calculated for each temperature difference using temperature dependence of the surface tension and density, Eqs. 4-5.

The numerical results for the static shape at $\Delta T = 0$ are presented in Fig. 4 for different volumes: $\mathscr{V} = 0.8, 0.9, 1.0$. The smaller the volume is, the large static deformation is with respect to the straight cylinder (dashed line). For the smallest volume studied, $\mathscr{V} = 0.8$, the main deviation is observed in the upper region of the narrow neck. As the volume increases, the maximum deviation occurrs at the bottom part (outward bulging). The maximum deviations from the straight shape at the upper part, is $\delta_1 = R_0 - F_{min}$, and at the bottom part, is $\delta_2 = F_{max} - R_0$. The results are summarized in Table 2. The net static deformation, $\delta_{net} = \delta_1 + \delta_2$, is about $600\,\mu m$ for $\mathscr{V} = 0.8$ and reduces down to $400\,\mu m$ for $\mathscr{V} = 1.0$

Table 2: Static and dynamic (as compared with static shape) deformations.

$\mathscr{V}$	δ_1	δ_2	δ_{net}	δ_1^{dyn}	δ_2^{dyn}	δ_{net}^{dyn}
	μm	μm	μm	μm	μm	μm
0.8	609	9	618	39	28	67
0.9	386	74	460	26	22	48
1.0	208	200	408	22	20	42

The dynamic deformation due to the flow was calculated with regular increase of applied temperature difference. The evolution of the dynamic deformation with increase of ΔT for $\mathscr{V} = 0.8$ is shown in Fig. 5 and for $\mathscr{V} = 1.0$ in Fig. 6. The dynamic deflections from the static shape are about

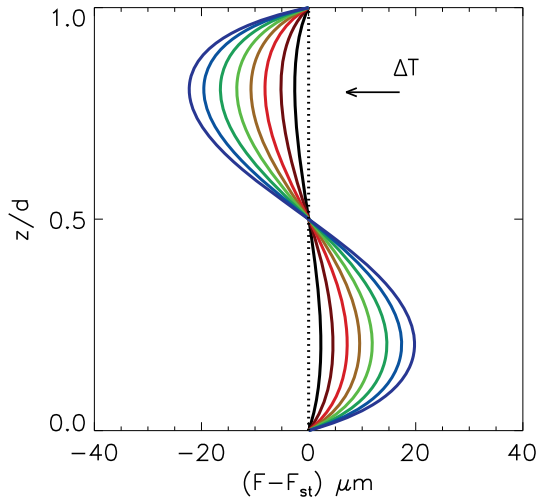

Figure 6: The evolution of free surface dynamic deformation with the increasing ΔT for $\mathscr{V} = 1.0$

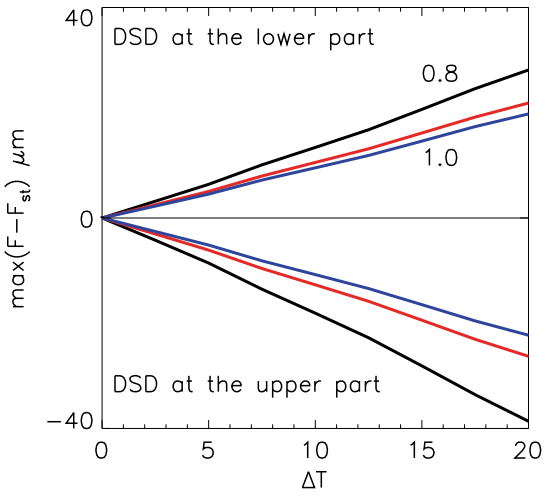

Figure 7: The progression of the dynamic surface deformation (DSD) with increasing ΔT for $\mathscr{V} = 0.8, 0.9, 1.0$, $Pr = 68, \Gamma = 1.23$

one order of the magnitude smaller than the static deformation. Due to the hardly visible deflections, they are shown on the scale in microns. Note that Fig.4 has scale in *mm*. For each volume (we also calculated $\mathscr{V} = 0.9$), similar tendency is observed in transformation of the free surface shape: the neck part bulges inward and bottom part bulges outward. For $\mathscr{V} = 0.8$ and $\mathscr{V} = 0.9$, the bulging is stronger at the upper part and for heavier liquid bridge, $\mathscr{V} = 1.0$, the outward bulging is larger at the bottom part. Again, as in the case of the static deformation, the deflections of the interface are larger for the smaller volume. In Table 2 the maximum value of the dynamic deviation from the static shape in the upper part, δ_1^{dyn}, near the bottom δ_2^{dyn} and net deformation $\delta_{net}^{dyn} = \delta_1^{dyn} + \delta_2^{dyn}$ are given for $\Delta T = 20\,K$. The experimental study indicated that this value of $\Delta T = 20K$ is very close to the threshold of oscillatory instability.

Actually, the progression of the dynamic deformation with applied temperature difference can be described by linear law, see Fig.7:

$$\Delta F = max|F - F_{static}| = \gamma \Delta T.$$

If ΔF is the maximum deformation at the neck region, then $\gamma_1(\mathscr{V}) < 0$ and ΔF is a decreasing function of ΔT. If ΔF is the maximal deformation at the bottom part, then $\gamma_2(\mathscr{V}) > 0$ and ΔF is an increasing function of ΔT. The values of the coefficients γ_i are given in Table 3.

These linear dependencies allow us to estimate the magnitude of dynamic deformation near the onset of oscillatory convection. Surprisingly, for analyzed system at the threshold of instability, the net dynamic deformation does not depend on volume and in average is about $44\mu m$. Extrapolating these linear dependencies in Fig. 7 beyond $\Delta T = 20K$, one may estimate that $\delta_{net}^{dyn} = 62\mu m$ for $\mathscr{V} = 0.9$ at $\Delta T = 25.8$. These results are in excellent agreement with our previous experimental measurements, $\delta_{net}^{dyn} \approx 60 - 65\,\mu m$ for $\mathscr{V} = 0.883$ and $\Delta T = 25.8$, see Ferrera et al. (2007).

Table 3: The growth rate of dynamic deformation, ΔF, and their values at critical point.

$\mathscr{V}$	$-\gamma_1$	γ_2	δ_1^{cr}	δ_2^{cr}	δ_{net}^{cr}
			μm	μm	μm
0.8	1.85	1.0	27	15	42
0.9	1.3	1.1	23	20	43
1.0	1.1	1.4	20	26	46

The most significant outcome of this numerical study is that the static deformation at $\Delta T = 0$ is $\sim 500\mu m$, while the subcritical dynamic surface deformation at $\Delta T = \Delta T_{cr}$ is at least 10 times

smaller, e.g. $\sim 44\mu m$. The ratio $\delta_{dyn}/\delta_{static}$ increases slightly with volume and is equal to 0.07, 0.09, 0.11 for $\mathscr{V} = 0.8, 0.9, 1.0$, respectively. For considered system near the onset of instability, this ratio can be estimated as $\delta_{dyn}/\delta_{static} = O(Ca)$ with reasonable precision, while $Ca \approx 0.06$.

The dynamic deformation, which is caused by the oscillatory convection can only be captured using the full three-dimensional calculations. The next section of the paper will present results for the oscillatory deformations that were measured experimentally.

4 Experimental results

In order to measure sub-micron deformation of the interface, large magnification lenses were used, which led to a decrease in the field of view. One field of view covers about $800 \times 800\mu m$. To obtain the axial dependence of the interface deformation of the entire liquid bridge, the camera was sled down along the vertical axis during the experiment. Eight displacements of the CCD camera were needed to cover the whole height of the liquid bridge. At each displacement the camera was fixed so that the images at different displacements correspond to various time instants. Each camera displacement corresponds to about $500\mu m$, while the entire height of the liquid bridge is $3.6 - 3.7mm$. Hence, the neighbouring displacements are partly overlapping which allow control of the measurements and/or the verticality of the camera motion.

4.1 Static shape

The static shape of the isothermal liquid bridge, i.e. $\Delta T = 0$, was measured using eight displacements of the CCD camera. For each displacement, the experimental results are shown using different colors in Fig. 8. The raw data for different displacements did not fit perfectly, revealing the small tilt of the camera axis and occasional horizontal vibration of the camera. Multicolored curve in Fig. 8 is due to the processing of raw experimental records taking into account this imprecision. The original mismatch between the two first displacements is kept at the upper part in

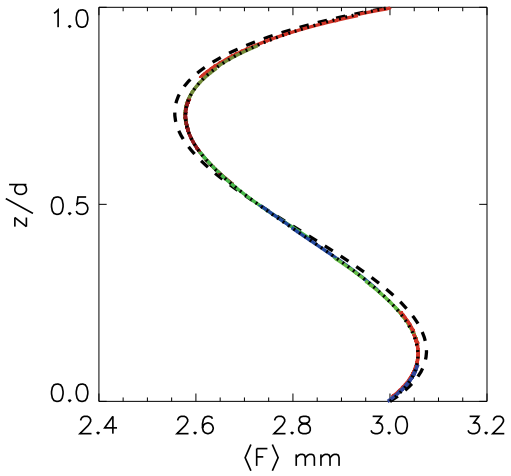

Figure 8: Experimental and numerical results. Dependence of free surface on height of the liquid bridge. The static shapes for the volume $\mathscr{V}_0 = 0.883$ and aspect ratio $\Gamma = 1.23$; experimental (multicoloured), numerical (dotted line) for $\Delta T = 0$ and $Bo = 6.25$ and numerical (dashed line) for $\Delta T = 25.8$ and $Bo = 6.82$;

Fig. 8, although it can be seen clearly only under magnification. The static shape was also calculated from the Young-Laplace equation, knowing the parameters of the system. For the prescribed aspect ratio and volume, the static shape was calculated at the reference temperature, $T = T_{cold}$, when the parameters of the 5 cSt silicone oil from Table 1 were used. This first numerical estimation was slightly different from the experimentally measured shape. Although the height and the volume of the liquid bridge were accurately measured, these measurements permit some tolerance. In addition, the deviation of physical properties of the working liquid from the tabulated values occur.

Numerical fit was employed to minimize the smallest horizontal distance from the experimental curve with respect to the surface tension and geometrical parameters. The result of these calculations is a profile, and more precise surface tension value and geometrical dimensions. The absolute differences are small but they become important for achieving accurate measurements. This procedure revealed that accuracy of the determination of the static shape is about $1 - 3\mu m$.

The numerical shape at $\Delta T = 0\,K$ after fitting is shown in Fig. 8 as the dotted line that corresponds to $Bo = 6.25$ and is not distinguishable from the multicoloured experimental curve without magnification.

Large amount of measurements were obtained for this particular liquid bridge volume $\mathscr{V}_0 = 0.883$ at $\Delta T = 25.8$. The static shape corresponding to this ΔT and, respectively, to the larger Bond number, $Bo_{st} = 6.82$, is shown in Fig. 8 by dashed line.

4.2 Supercritical dynamic deformations

As the applied temperature gradient is parallel to the interface, motion from the hot to the cold region appears for any non-zero value of ΔT. When the temperature difference between the disks exceeds the critical value, $\Delta T > \Delta T_{cr}$, unique for a given set of parameters, the flow is three-dimensional and/or unsteady. Generally, two hydrothermal waves propagating in opposite directions bifurcate from two-dimensional state at the critical point. They result in standing or traveling wave depending on the ratio of their amplitudes. As a rule, for the system under consideration with volumes $\mathscr{V} = 0.8, 0.9, 1.0$ a traveling wave with azimuthal wave number $m = 1$ was observed at the threshold of instability.

The critical temperature difference was identified by two quantities: oscillations of the free surface and the temperature on five thermocouples. Both quantities exhibit the same ΔT_{cr}.

The critical frequency of the interface oscillation was calculated by averaging over the whole interface. Fourier analysis was used for processing the time-dependent signals of the thermocouples. The values of ΔT_{cr} and f_{cr} for different volumes are given in Table 4.

Table 4: The critical parameters for $\Gamma = 1.23$ and $Pr = 68$.

$\mathscr{V}$	ΔT_{cr}	f^{cr}
	K	Hz
0.8	14.71	0.336
0.9	18.02	0.415
1.0	18.44	0.403

Oscillatory motion starts at a critical value of ΔT and causes oscillation of the interface. One of the goals of this study was to examine the development of oscillation amplitude above the critical point. Partly such analysis was performed using the measurements in the first field of view, i.e. near the hot corner.

For each examined temperature difference the six images of the interface, corresponding to the six equidistant time intervals over the period, were analyzed. The oscillation amplitudes were calculated from these snapshots for each vertical coordinate z.

The z -dependence of the oscillation amplitude near the hot corner for $\mathscr{V} = 0.8$ is shown in Fig. 9 where different colours correspond to various ΔT above the threshold of instability. Just above the critical point, the amplitude gradually increases over the entire height of the liquid bridge. First four curves show similarity with self-similar regime of propagation. In general, such behaviour corresponds to the flow pattern when hydrothermal wave propagates azimuthally. When the system is above the threshold of instability by about 17%, the amplitude growth starts decelerating and a pronounced peak appears on the amplitude shape $A(z)$. The amplitude profiles are very smooth and the peak of amplitude of each profile is located very close to the upper rigid wall, $d - z \approx 120\mu m$. When the system is close to the critical point the amplitude has sub-micron size and our digital optical imaging technique allows us such measurements. When sustained oscillations are established, the amplitude of oscillations attains $\sim 1\mu m$ for $\mathscr{V} = 0.8$.

Using eight successive displacement of the CCD camera, the oscillation amplitude over the entire height of the liquid bridge was measured for $\mathscr{V} = 0.883$ and $\varepsilon = 55.4$ ($\Delta T_{cr} = 16.6$). Using various symbols at different displacements, the results are presented in Fig. 10. The amplitude of oscillations exhibits a strong z-dependence. The largest variation of the amplitude takes place at the upper part when $z/d > 0.4$. The amplitude reaches a maximum at $z/d \approx 0.9$ or, in other words, $d - z \approx 350 - 370\mu m$. The maximum is located noticeably lower than in the previous case

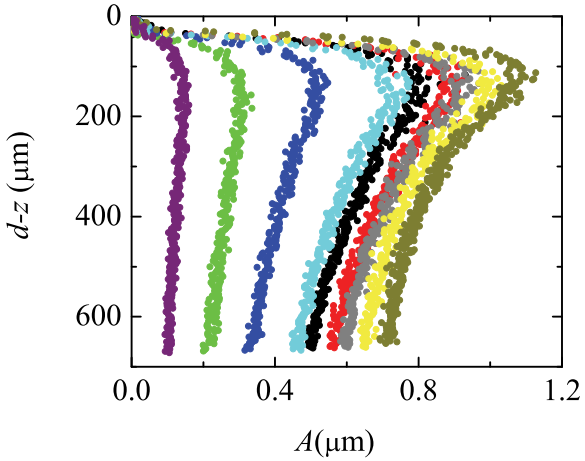

Figure 9: z-dependence of oscillations amplitude near the hot corner for $\mathscr{V} = 0.8$, when $\Delta T_{cr} = 14.71$. Parameter $\varepsilon = 100 \cdot (\Delta T - \Delta T_{cr})/\Delta T_{cr}$ characterizes the supercriticality (percentage above the threshold). Different colors correspond to the various applied temperature differences: (from the left to the right) $\varepsilon =$ 0., 3.18, 9.70, 17.64, 22.32, 27.17, 32.01, 39.44 and 46.85

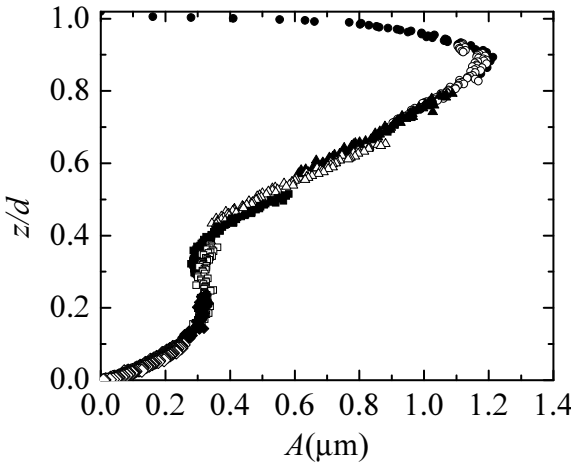

Figure 10: z-dependence of oscillations amplitude over the whole height of the liquid bridge, $\mathscr{V} = 0.883$ and $\varepsilon = 55.4$ ($\Delta T = 25.8$ while $\Delta T_{cr} =$ 16.6). Various symbols correspond to the results from the different displacement of the CCD camera

$\mathscr{V} = 0.8$, see Fig. 9, but still very close to the hot wall. The maximum measured amplitude for these parameters of the system is about 1.2 μm.

Moving down from the hot wall to $z/d \approx 0.4$ the amplitude sharply decreases. The relatively large region where the amplitude practically does not change occurs when $0.2 < z/d < 0.4$. Below, closer to the cold disk, the free surface oscillations quench and it results in diminishing of the amplitude. Actually, the z-dependence of the oscillation amplitude $A(z)$ is strongly related to the temperature deviations from mean value, e.g. $[T - T_{mean}](z)$. The stronger temperature variation is, the larger free surface deformation is.

The evolution of two different quantities, the amplitude of the free surface and of the temperature oscillations, with the increase of applied temperature difference is shown in Figure 11. The amplitude of temperature oscillations at the thermocouple, closest to the examined silhouette in azimuthal direction, is presented by filled symbols while the amplitude of the interface oscillations is shown by open symbols. The green squares and red circles correspond to $\mathscr{V} = 0.8$ and 0.9, respectively. The amplitude of the free surface oscillations was measured at the distance $d - z \approx 500\,\mu m$ from the upper disk for each ΔT. The thermocouples are positioned much below, $d - z \approx 1260\,\mu m$ and inside the liquid $r/R_0 \approx 0.75$. By chance both quantities can be represented using the same vertical scale where temperature is measured in K degrees and the interface deflection in microns.

The same critical temperature differences are identified by both quantities, i.e. $\Delta T_{cr} = 14.7\,K$ for $\mathscr{V} = 0.8$ and $\Delta T_{cr} = 18.0\,K$ for $\mathscr{V} = 0.9$. In addition both amplitudes (temperature and interface oscillations) grow with increase of ΔT in the same manner. For $\mathscr{V} = 0.8$ both profiles demonstrate similar dynamical trends for all examined ΔT. For the larger volume, $\mathscr{V} = 0.9$, the small difference in the dynamic behavior appears at $\Delta T > 23K$ (or when $\varepsilon > 28$). It may be a sign of some additional transitions which occur on the free surface.

Our results are in good agreement with the measurements by Nishino & Yoda (2000) who obtained dynamic surface deformations of about $1\mu m$ in experiments with 5 cSt silicone oil. They also indicated that the maximum of the oscillations amplitude was located at the upper part of

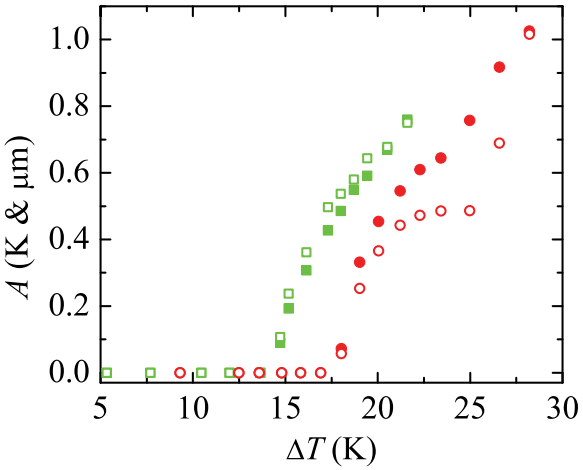

Figure 11: Amplitudes of the free surface deformations at $d-z \approx 500\mu m$ (open symbols) and of the temperature oscillations at thermocouple (filled symbols) vs. the applied temperature difference ΔT. The green squares and red circles corresponds to $\mathscr{V} = 0.8$ and 0.9 respectively.

the liquid bridge. It seems that such shape of the amplitude profile, when maximum is located near the hot wall, corresponds to the hydrothermal traveling wave with azhimutal wave number $m = 1$.

To summirize the most important result of this section, one may notice that the supercritical oscillatory deformations are one or two order of magnitude smaller that stationary dynamic deformation, i.e. $\delta_{os} \sim 1\,\mu m$. Consequently, comparison of the oscillatory deflections with the static deformation indicates that their ratio is $\delta_{os}/\delta_{st} \sim 1/500 \approx 0.002 \sim O(C)$. As it is seen from Fig. 9, this ratio depends how far the system is above the critical point.

5 Conclusions

Static and dynamic free surface deformations (DSD) induced by buoyant and thermocapillary convection in liquid bridges of $5\,cSt$ silicone oil are studied experimentally and numerically. The final supercritical shape of the free surface is a result of the static shape with superimposed subcritical stationary and supercritical oscillatory dynamic deformations. The study was performed in three steps for different initial volumes: (1) the static shape was measured experimentally and the physical properties of liquid were fine-tuned by comparing the measured shape with the computed one; (2) subcritical deformations due to stationary convection were studied numerically; (3) supercritical dynamic deformations due to oscillatory convection were measured experimentally.

The study was performed for different liquid bridge volumes: $\mathscr{V} = 0.8, 0.883, 0.9, 1.0$. The important result of the numerical study is that the static deformation at $\Delta T = 0$ is $\sim 500\mu m$, while the subcritical dynamic surface deformation at $\Delta T = \Delta T_{cr}$ is at least 10 times smaller, e.g. $\sim 44\mu m$. The ratio $\delta_{dyn}/\delta_{static}$ increases slightly with volume and near the onset of instability, this ratio can be estimated as $\delta_{dyn}/\delta_{static} \sim 10^{-1} = O(Ca)$.

The most significant result of the experimental study is that the supercritical oscillatory deformations are one or two order of magnitude smaller that stationary dynamic deformation. The maximum amplitude of the oscillations around their mean value (i.e. stationary dynamic deformation) is $\delta_{os} \sim 1\,\mu m$. The comparison of the supercritical oscillation amplitude with the static deformation leads to $\delta_{os}/\delta_{static} \sim 10^{-3} \approx O(C)$. Note that $C = Ca/Re$ and in the superctitical regime $Re >> 1$. Thus, to capture the oscillatory deformation in three-dimensional calculations the straightforward expansion in the limit of small Ca could be not sufficient.

Acknowledgement: We would like to thank Dr. Kenol Jules, NASA Johnson Space Center, Houston for the useful discussions.

References

Chen, Q.S.; Hu, W.R. (1998): Influence of liquid bridge volume on instability of floating half zone convection. *Int. J. Heat and Mass Transfer*, **42**, 825.

Ermakov M.K.; Ermakova M.S. (2004): Linear-stability analysis of thermocapillary convection in liquid bridges with highly deformed free surface. *J. Cryst. Growth*, **266**, 160.

Ferrera, C.; Cabezas, M.G.; Montanero J.M. (2006): An experimental analysis of the linear vibration of axisymmetric liquid bridges. *Phys. Fluids*, **18**, 082105.

Ferrera C.; Mialdun A.; Shevtsova V.; Cabezas M.G.; Montanero J.M. (2007): Experimental analysis of the dynamic surface deformation in liquid bridges, submitted to *JFM*.

Hu, W.R.; Shu, J.Z.; Zhou, R; Tang, Z.M. (1994): Influence of liquid bridge volume on the onset of oscillation in floating zone convection. *J. Cryst. Growth*, **142**, 379.

Kamotani, Y.; Ostrach, S., Masud, J. (2000): Microgravity experiments and analysis of oscillatory flow in cylindrical containers. *J. Fluid Mech.*, **410**, 211.

Kamotani Y.; Matsumoto S.; Yoda S. (2007): Recent developments in oscillatory Marangoni convection. *FDMP: Fluid Dynamics & Materials Processing*, **2**, 147.

Kuhlmann, H. C.; Nienhuser, C. (2002): Dynamic free-surface deformations in thermocapillary liquid bridges. *Fluid Dynamic Research*, **31**, 103.

Lappa, M.; Savino, R.; Monti, R. (2001): Three-dimensional numerical simulation of Marangoni instabilities in non-cylindrical liquid bridges in microgravity. *Int. J. of Heat Mass Transfer*, **44**, 1983.

Nienhüser, C.; Kuhlmann, H. C. (2002): Stability of thermocapillary flows in non-cylindrical liquid bridges. *J. Fluid Mech.*, **458**, 35.

Nishino, K.; Yoda, Sh. (2000): The role of dynamic surface deformation in oscillatory Marangoni convection in liquid bridge of high Prandtl number. In: Inokuchi, H.(Ed.), Marangoni convection Modeling Research, NASDA Technical Memorandum, NASDA, No. TMR-000006E, 43.

Shevtsova, V.M. (2005): Thermal convection in liquid bridges with curved free surfaces: benchmark of numerical solutions. *J. Crystal Growth*, **280**, 632.

Shevtsova, V.M.; Ermakov, M.K.; Ryabitskii E.; Legros, J.C. (1997): Oscillations of a liquid bridge free surface due to the thermal convection. *Acta Astonautica*, **41**, 471.

Shevtsova, V.M.; Legros, J.C. (1998): Thermocapillary motion and stability of strongly deformed liquid bridges. *Phys. Fluids*, **10**, 1621.

Shevtsova, V.M.; Mojahed, M.; Legros J. C. (1999): The loss of stability in ground based experiments in liquid bridges. *Acta Astronautica*, **44**, 625.

Sim B.C.; Zebib A. (2002): Thermocapillary convection in liquid bridges with underformable curved surfaces, *AIAA J. Thermophysics and Heat transfer*, **16**, 553.

Shu, J.Z.; Yao, Y.L.; Zhou, R.; Hu, W.R. (1994): Experimental study of free surface oscillations of a liquid bridge by optical diagnostics. *Microgravity Sci. Technol.*, **VII/2**, 83.

Sumner, L.B.S.; Neitzel, G.P.; Fontaine J.-P.; Dell'Aversana P. (2001): Oscillatory thermocapillary convection in liquid bridges with higly deformed free surfaces: experiments and energy-stability analysis. *Phys. Fluids*, **13**, 107.